Check for updates

Nanoparticles Hot Paper

How to cite: *Angew. Chem. Int. Ed.* **2021**, *60*, 12591 – 12596
International Edition: doi.org/10.1002/anie.202103110
German Edition: doi.org/10.1002/ange.202103110

Truly Monodisperse Molecular Nanoparticles of Cerium Dioxide of 2.4 nm dimensions: A $\{Ce_{100}O_{167}\}$ Cluster

*Bradley Russell-Webster, Javi Lopez-Nieto, Khalil A. Abboud, and George Christou**

Abstract: *Ultra-small nanoparticles of CeO_2 obtained in molecular form, so-called molecular nanoparticles, have been limited to date to a family whose largest member is of nuclearity Ce_{40} with a $\{Ce_{40}O_{58}\}$ core atom count. Herein we report that a synthetic procedure has been developed to the cation $[Ce_{100}O_{149}(OH)_{18}(O_2CPh)_{60}(PhCO_2H)_{12}(H_2O)_{20}]^{16+}$, a member with a much higher Ce_{100} nuclearity and a $\{Ce_{100}O_{167}\}$ core that is more akin to the smallest ceria nanoparticles. Its crystal structure reveals it to possess a 2.4 nm size and high D_{2d} symmetry, and it has also allowed identification of core surface features including facet composition, the presence and location of Ce^{3+} and H^+ (i.e. HO^-) ions, and the binding modes of the ligand monolayer of benzoate, benzoic acid, and water ligands.*

Introduction

Cerium dioxide nanoparticles (CNPs, nanoceria) have been under intense study for many years in a wide variety of applications, including industrial catalysis of different types,[1–4] new energy technologies,[5–7] and more recently for very small CNPs (< 20 nm) biomedical applications.[8–11] Their significant activity even near ambient temperatures is facilitated by their nanoscale dimensions, Ce^{3+}/Ce^{4+} redox ability, oxygen mobility within their fluorite lattice, and the formation on their surface of oxygen-vacancy defect sites and attendant Ce^{3+} ions.[1,2,5,12] Within the biomedical arena, the high reactivity of CNPs at ambient temperatures is permitting many important applications to be developed, such as scavenging of reactive oxygen species (ROS),[9,10,13,14] but activity vs. toxicity questions abound and these properties clearly depend on CNP size, shape, surface composition (such as Ce^{3+}/Ce^{4+} ratios), and other factors.[15–18] However, the range of size, shape, Ce^{3+} content, and surface variations characteristic of nanoparticle samples makes it very challenging to answer these questions and come to conclusions about how such structural factors influence these properties.

With the above in mind, we have recently initiated a molecular bottom-up approach to ultra-small (< 3 nm) CNPs that targets their synthesis as molecular clusters to take advantage of the molecular properties of true monodispersity (single size), solubility, and crystallinity, the latter allowing structural characterization to atomic precision by single-crystal X-ray crystallography.[19–21] We first developed synthetic procedures in pyridine (py) or py/water (10:1 v/v) to a family of Ce-oxo clusters with primarily carboxylate ligation and formulas $[Ce_{24}O_{28}(OH)_8(PhCO_2)_{30}(py)_4]$ (**1**; Ce_{24}), $[Ce_{38}O_{54}(OH)_8(EtCO_2)_{36}(py)_8]$ (**2**; Ce_{38}) and $[Ce_{40}O_{56}(OH)_2(MeCO_2)_{44}(MeCO_2H)_2(py)_4]$ (**3**; Ce_{40}), and core dimensions up to 1.6 nm for Ce_{40} **3**.[19] Their crystal structures confirmed the cores to possess the fluorite structure of bulk CeO_2, namely alternating layers of eight-coordinate cubic Ce^{4+} and tetrahedral O^{2-} ions, and thus these molecular clusters truly are small pieces of CeO_2 with a surface organic monolayer of carboxylate and py ligands; we now favor the name molecular nanoparticles (MNPs) for such species.[19] They have also allowed crucial information to be obtained to atomic resolution of surface features important to the application of CNPs in catalysis and elsewhere, such as the facet composition, organic ligand binding modes, location of Ce^{3+} and H^+ ions, O vacancies, and others, information extremely difficult if not impossible to obtain for CNPs.

The above results provided an excellent foundation for the new project but what was now needed was a breakthrough into distinctly higher sizes/nuclearities more analogous to those of ultra-small CNPs of 2–10 nm dimensions. The different nuclearities of **1**–**3** had resulted from a systematic study of the influence of the carboxylate identity on the product, with Ce_{24}, Ce_{38} and Ce_{40} being obtained from the use of benzoate, propionate and acetate, respectively.[19] However, further exploration of various carboxylates all led to derivatives of **1**–**3** or smaller nuclearities such as Ce_6, Ce_{16}, and Ce_{19}.[20] The same was observed when halides were included in the reaction, giving for example a Ce_{20} product with Cl^- on the surface.[21] We thus turned our attention to systematically exploring the influence of other reaction parameters, and one of these has been the py ligands that we have always found binding to hexagonal (111) facets and never to (100) or (110) facets, the other two low-index thermodynamically stable facets of CNP's and molecular nanoparticles.[1,2,22,23] DFT calculations have found that these decrease in stability (surface free energy) in the order (111) > (110) > (100), consistent with catalytic activity which follows the opposite trend.[1,24–27]

Since the py ligands in **1**–**3**[19] are capping (binding at the center of) the hexagonal (111) facets, which also contain three μ_3-O^{2-} ions (Figure 1), it seemed logical to wonder whether inhibiting the binding by py might allow additional Ce ions to bind to the μ_3-O^{2-} ions, leading to further growth in that direction and increasing the overall nuclearity of the MNP. Viewing the capping by py in space-filling mode reveals the py

[*] B. Russell-Webster, J. Lopez-Nieto, Dr. K. A. Abboud, Prof. Dr. G. Christou
Department of Chemistry, University of Florida
Gainesville FL, 32611-7200 (USA)
E-mail: christou@chem.ufl.edu
Supporting information and the ORCID identification number(s) for the author(s) of this article can be found under: https://doi.org/10.1002/anie.202103110.

 © 2021 Wiley-VCH GmbH

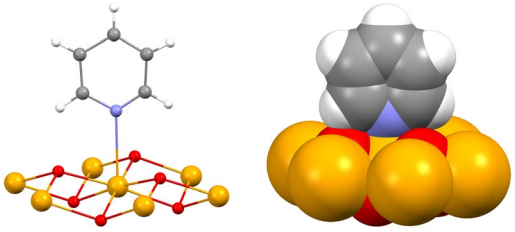

Figure 1. A pyridine molecule capping the hexagonal (111) facet of a Ce_x molecular nanoparticle, viewed in ball-and-stick and space-filling mode, emphasizing that functionalizing the py *ortho* position should inhibit py binding. Ce^{IV} gold, O red, N blue, C gray, H white.

to be closely nestled on the (111) facet surface and that steric hindrance from substituents larger than H in the *ortho* position(s) could inhibit its binding. We thus explored whether the use 2-Me-py as the reaction co-solvent might alter the product nuclearity, and this has successfully resulted in the desired breakthrough with the synthesis of a Ce_{100} MNP of ≈2.4 nm dimensions.

Results and Discussion

The reaction system developed was a slightly modified version of that used by Mitchell et al. to prepare **1**–**3**.[19] Thus, a solution of $(NH_4)_2Ce(NO_3)_6$, $Ce(NO_3)_3$ and $PhCO_2H$ in a 1:4:24 molar ratio in 2-Me-py/H_2O (10:1 v/v) was stirred for 30 minutes to give a brown solution, and this was layered with acetone (20 mL) and maintained undisturbed at ambient temperature for about 8 weeks. Brown crystals containing the $[Ce_{100}O_{149}(OH)_{18}(O_2CPh)_{60}(PhCO_2H)_{12}(H_2O)_{20}]^{16+}$ (**4**) cation as the **[4]**$(PhCO_2)_8(NO_3)_8{\cdot}4\,Me_2CO{\cdot}x$(solv) salt slowly grew and were isolated in 20% typical yield. In the absence of $(NH_4)_2Ce(NO_3)_6$, the same product was obtained but with a longer crystallization time of 12 weeks.

As control experiments, we carried out the identical reactions but with py, 3-Me-py, and 4-Me-py, and they all gave the analogous Ce_{24} clusters **5**–**7**, respectively, containing py-based ligands and consistent with previous observations that a benzoate and py ligand shell favors Ce_{24} clusters. The products were confirmed by their elemental analyses and very similar FT-IR spectra to each other (Supporting Information, Figure S1) and to those of **5** prepared previously under slightly different conditions and characterized by X-ray crystallography (Supporting Information, Figure S2);[20] **5** is essentially identical to **1**[19] except that it contains three Ce^{3+} ions whereas **1** contains two Ce^{3+}. The elemental analyses also confirmed that there are four pyridines in **5**–**7**, the same as the number of hexagonal (111) facets, indicating their capping of all the latter. These control experiments all giving Ce_{24} products whereas 2-Me-py under identical conditions gives **4** support the role of the 2-Me substituent in increasing the nuclearity by inhibiting 2-Me-py binding; note that there are no 2-Me-py ligands anywhere in the Ce_{100} cation **4**. Further experiments are underway to see whether other 2-functionalized pyridine solvents also lead to **4** or other high nuclearity products.

[4]$(PhCO_2)_8(NO_3)_8{\cdot}4\,Me_2CO{\cdot}x$(solv) crystallizes in tetragonal space group $P4_2/nmc$ with $^1/_8$ of the cation in the asymmetric unit.[28] A summary of the structure of cation **4** (Figure 2)[28] is given here and expanded upon later:

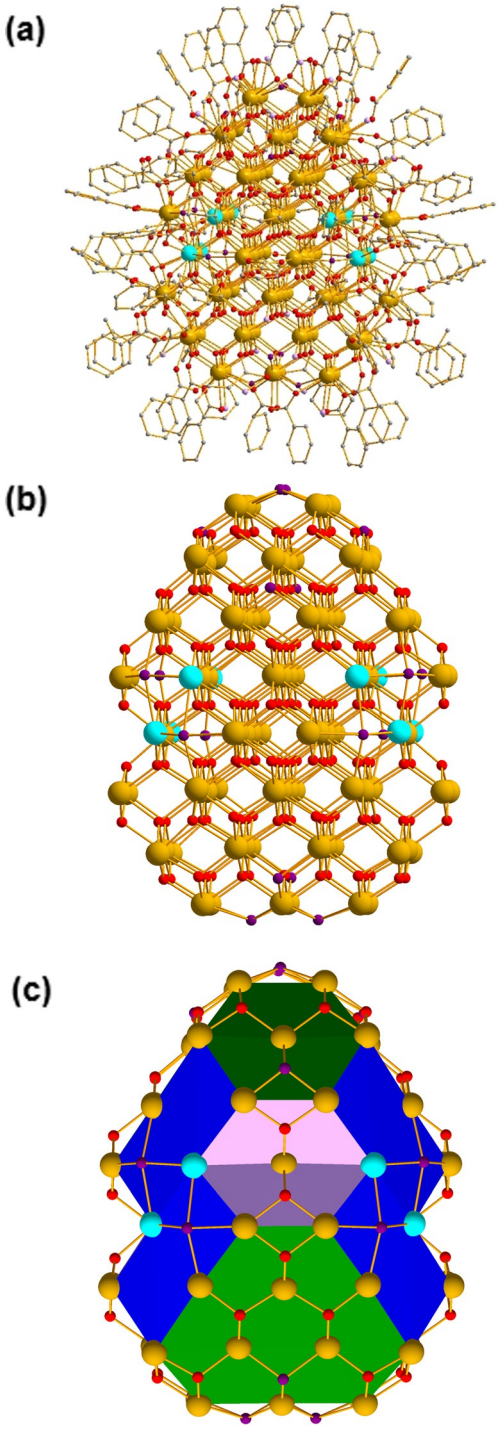

Figure 2. The structure of cation **4**.[28] a) The complete structure, excluding ligand disorder; b) the $\{Ce_{100}O_{149}(OH)_{18}\}^{76+}$ core, slightly rotated about the horizontal axis compared with (a) to better show the layered structure; and c) the core from the viewpoint of (a) showing the surface facets. Ce^{IV} gold, Ce^{III} light blue, O red, OH purple, H_2O lilac, C gray. H atoms have been omitted for clarity. Facets: (111) green, (110) violet, (100) blue.

© 2021 Wiley-VCH GmbH

(i) the Ce_{100} cation **4** has crystallographically imposed D_{2d} point group symmetry, ignoring ligand disorder. From the viewpoint of Figure 2, the vertical axis is the unique C_2 and the S_4 axis.

(ii) From the same viewpoint, the Ce_{100} core consists of an A:B:C:D:D:C:B:A eight-layer arrangement with A = 6, B = 12, and C = D = 16 (Figure S3), separated by seven layers of tetrahedral oxide ions to give a total Ce/O atom count of 267 (including the OH^- oxygen atoms).

(iii) The core thus has the fluorite structure of bulk CeO_2, with approximate dimensions of $2.4 \times 2.0 \times 2.0$ nm. There are 28 body Ce atoms in the core, the rest are on the surface. Hence **4** is of a similar size to large nanoclusters of Mo,[29] Ag[30] and Au[31–33] that have been reported.

(iv) Ce oxidation states and O protonation levels were determined by bond valence sum (BVS) calculations, revealing a $Ce^{3+}{}_8Ce^{4+}{}_{92}$ situation and 18 surface OH^- ions.

(v) All three low-index facets of CNPs, namely (111), (110) and (100), are present in **4**. Only the Ce_{40} (**3**) has previously exhibited all three types.

(vi) All eight Ce^{3+} ions are on the surface and all are in (100) facets, as also found in almost all the smaller MNPs, the exception being Ce_{19} where a Ce^{3+} is located on a Ce_2 edge joining two (111) hexagons.

(vii) The capping ligands on (111) facets are H_2O or $PhCO_2H$.

(viii) Most of the $PhCO_2^-/PhCO_2H$ binding modes are the same as seen previously in the smaller MNPs, except for two new μ_2-$PhCO_2H$ and μ_4-$PhCO_2^-$ bridging modes (Figure S4).

We have shown elsewhere the power of BVS calculations not just to identify the location of Ce^{3+} ions from Ce BVS but also the position of surface H^+ (that is, OH^-) by their influence on the O BVS values,[34,35] information extremely challenging to obtain on CNPs. The resulting conclusion is 92 Ce^{4+}, 8 Ce^{3+}, 149 O^{2-}, 18 OH^-, 60 $PhCO_2^-$, 12 $PhCO_2H$, and 20 H_2O in **4** (Supporting Information, Tables S2 and S3),[34,35] leading to an overall charge of 16+. Counterions could not be located due to extensive disorder of anions and most solvent molecules in voids between the protein-sized cations but elemental analysis of vacuum-dried material indicated the anions to be 8 $PhCO_2^-$ and 8 NO_3^- (see the Supporting Information). Only four Me_2CO solvent molecules (O121) are ordered because of their strong H-bonding with surface μ_3-OH^- (O20···O121 = 2.472 Å) and nearby capping H_2O (O48···O121 = 2.382 Å) ligands on the cation.

Most observations from the smaller MNPs are retained in the structure of **4** including: neutral ligands capping the (111) facets (H_2O or $PhCO_2H$); ligands adopting particular binding modes at specific facet intersections; and μ_4-OH^- ions capping the Ce_4 squares that represent the (100) facets. These consistencies across the Ce/O MNP family highlight the overall validity of earlier observations and conclusions. However, there are also a few new features in **4** not seen previously in the smaller clusters, including Ce^{3+} ions coordinated to a greater number of O^{2-} ions (4 vs. 2 in smaller MNPs), new coordination modes for carboxylates and carboxylic acids, and larger surface area (111) and (100) facets.

The last point is the most obvious effect of increasing the nuclearity as the larger surface area accommodates larger facets. There are two sizes of (111) facets (Figures 2c and 3), four Ce_7 single hexagons, the most common facet in the Ce_{40} and smaller clusters, and four larger Ce_{12} isogonal hexagons. Pairs of different (111) types are separated by a trench-like (110) facet on the four sides of **4**. With no bound 2-Me-py in **4**, all (111) facets are capped by water and $PhCO_2H$ ligands (Supporting Information, Table S3). The single water ligands (O48) capping each Ce_7 (111) facet are those H-bonding with lattice acetone, whereas the Ce_{12} (111) facets each possess three capping ligands, two waters and one $PhCO_2H$; one of the capping waters (O55) is H-bonded to a nearby bridging $PhCO_2H$ ligand (O55···O51 = 2.746 Å), whereas the capping $PhCO_2H$ (O52) forms an intramolecular H-bond between its unbound -OH (O53) arm and the μ_3-OH^- (O27) in the facet (O27···O53 = 2.639 Å), (Figure 3).

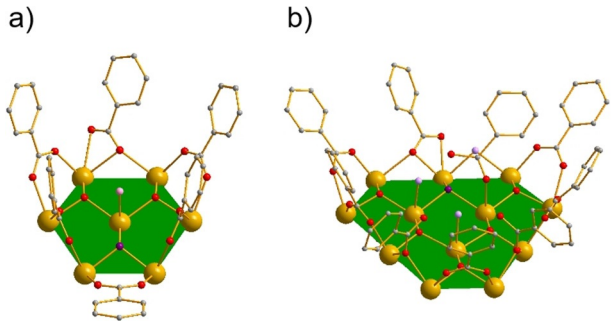

Figure 3. Two types of (111) facets present in **4**. a) The Ce_7 hexagonal facet common in other Ce/O molecular nanoparticles, and b) the larger Ce_{12} facet. Ce^{IV} gold, O red, OH purple, H_2O lilac, C gray. H atoms have been omitted for clarity. Facet (111): green.

The surface is completed by six (100) facets, and again we see two sizes: two smaller double-square (100) facets (as seen also in Ce_{40}) at the two ends (top and bottom of Figure 2c, and Figure 4a), and four larger quadruple-square (100) facets (never seen before in smaller clusters) on the sides (Figure 4a). As also seen for most of the (100) facets in other Ce/O MNPs,[19,20] 12 of the 20 Ce_4 (100) squares in **4** are bridged by μ_4-OH^- ions that are weakly bound (Ce···O = 2.632–2.819 Å); we previously called these "lids" on the Ce_4 squares and proposed them as possibly corresponding to the O-vacancy sites of CNPs. The remaining 8 Ce_4 squares are bridged by η^2:η^2:μ_4-$PhCO_2^-$ groups (Figure 4a,b), an unprecedented binding mode in all previous Ce/O clusters where it is sterically prevented by the tighter packing of the ligand shell around smaller (100) facets (Supporting Information, Figure S4); this is a rare bridging mode in general for carboxylates. Also not seen previously are monoatomically bridging μ-$PhCO_2H$ (Figure 4) and μ-OH_2 ligands on the larger and smaller (100) facets, respectively, the latter bridging on (100)(110) facet intersections.

 © 2021 Wiley-VCH GmbH

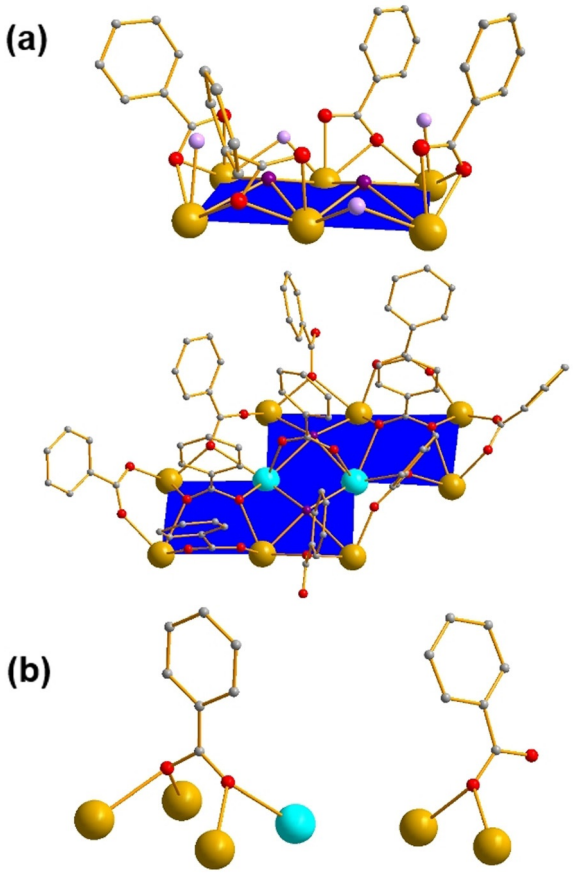

Figure 4. a) The (100) facets present in **4**, the smaller Ce_6 double-square and larger Ce_{10} quadruple-square facets; and b) the new carboxylate bridging modes seen in **4**. Ce^{IV} gold, Ce^{III} light blue, O red, OH purple, H_2O lilac, C gray. H atoms have been omitted for clarity. Facet (100): blue.

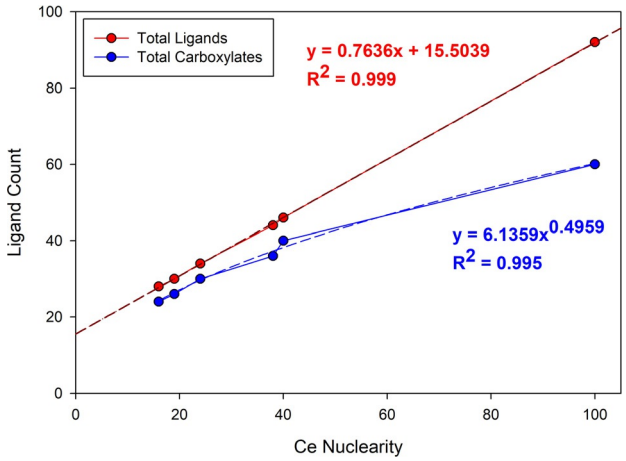

Figure 5. Plots of Ce nuclearity vs. the total ligands (red ●) and the total carboxylates (blue ●). Fits of the data (red and blue dashed lines) gave the indicated equations in the corresponding colors.

The increased cerium nuclearity range now available with the synthesis of **4** has allowed a useful analysis of the monolayer of $PhCO_2^-/PhCO_2H/H_2O$ ligands. Excluding the Ce_6 clusters, which are too small to be reasonably compared with the rest, a plot of Ce nuclearity vs. the total ligand count (excluding μ_3-HO^- ions of the core surface) (Figure 5) shows a linear relationship, whereas the number of charged carboxylate ligands shows a distinct curvature, that is, the fraction of charged carboxylate ligands in the total is decreasing. The former is very interesting and a fit to a linear relationship (red dashed line and equation in Figure 5) gives a slope of 0.76 ligands/Ce, or 3 ligands per 4 Ce. As the Ce nuclearity increases the difference between the two plots increases, indicating a greater proportion of neutral ligands and rationalizing the high charge of the cation. In other words, cation **4** has a high number of surface H^+ in $PhCO_2H$ and H_2O groups. We feel the charged vs. neutral ligands factor is likely not nuclearity-defining, however, since this primarily affects the cluster charge, but the linear relationship between total ligands and nuclearity offers a predictive utility. First, to assess the uncertainty in such a model, the formulas for the Ce_{38} and Ce_{100} were omitted in turn from the fit and the obtained relationship used to predict their formulas. The results (Supporting Information, Figure S5 and Table S4) predicted 45 and 90 total ligands for Ce_{38} and Ce_{100}, respectively, compared with 44 and 92 for the synthesized compounds. Applying now the full fit equation of Figure 5 gives the predicted formulations of Table 1 for some arbitrary nuclearities both smaller and larger than **4**. The important columns are the first two, because the charged:neutral ligand ratio is likely to be dependent on the morphology and resulting facet composition of the large clusters since the (111) facets will be a main location for neutral capping ligands; we note that 16 (50%) of the neutral ligands in **4** are at such positions. MNP morphologies with greater or lesser coverage with (111) facets should therefore affect this ratio. For example, the Ce_{20} shows a high surface coverage of (100) facets and has a RCO_2^-:Ce ratio (1.1:1) similar to that of the larger Ce_{38} that displays predominantly (111) facets (Table 1).[21] Note also that DFT calculations have concluded that H_2O coordination becomes more favorable with greater H_2O coverage,[36] consistent with our observations and predictions that the fraction of neutral ligands increases with nuclearity.

We now consider the Ce/O core of **4**. The lattice constant (*a* axis length) for bulk CeO_2 is 0.541 nm, corresponding to a Ce··Ce distance of 0.383 nm (3.83 Å). Most[37–40] but not all[41] experimental studies have concluded that the lattice constant increases with decreasing CNP size, suggesting increasing Ce··Ce distances in the Ce_4 planes that represent

Table 1: Predicted formulas of Ce_x molecular nanoparticles using the fitting equations in Figure 5.

x[a]	Total ligands	RCO_2^- ligands	Neutral ligands	Ligand:Ce ratio
38[b]	44	36	8	1.16
40[b]	50	46	4	1.25
52	56	44	12	1.08
80	77	54	23	0.96
100[b]	92	60	32	0.92
125	111	67	44	0.89
150	130	74	56	0.87
200	168	85	83	0.84

[a] *x* = Ce nuclearity. [b] The values for Ce_{38} (**2**), Ce_{40} (**3**)[19] and cation **4** are included for comparison.

© 2021 Wiley-VCH GmbH

the axes of ceria, whereas a computational study by DFT of small octahedral pieces of ceria up to $\{Ce_{85}O_{100}\}$ indicated the opposite.[42] This lattice anomaly has been assigned to increasing surface Ce^{3+} content and attendant O-vacancies with decreasing CNP size, as well as variations in synthesis, particle morphology, and drying conditions.[41]

The nearest-neighbor Ce··Ce distances in bulk ceria are 3.83 Å. In Figure 6 are plotted average nearest-neighbor Ce··Ce distances vs. Ce nuclearity for three MNPs, **1** (Ce_{24}), **2** (Ce_{38}) and **4** (Ce_{100}), all sub-2.5 nm species containing 2, 0, and 8 Ce^{3+} ions, respectively.[19] Since we have crystal structures,

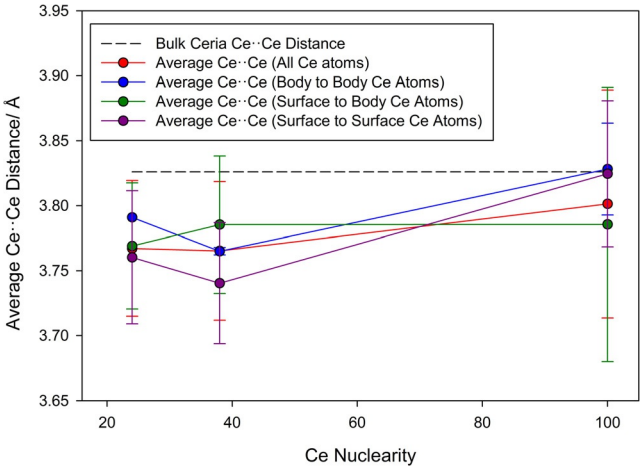

Figure 6. Plots of average Ce···Ce distance vs. Ce nuclearity. The bars indicate the standard deviations of that category.

we also plotted sub-groups of Ce··Ce distances, as indicated. The average Ce··Ce distances in all categories for Ce_{24} and Ce_{38} are less than in bulk ceria, and all increase or stay the same in going to Ce_{100} (**4**). The latter is the only one big enough to have a significant number of body Ce atoms (28), and for these the average Ce··Ce distance is 3.83 Å, the same as in bulk ceria. Interestingly, this is also true for the Ce··Ce atoms on the surface. Given that this is small set of compounds in this nuclearity range, and that their morphologies, facet composition, and Ce^{3+} content differ, we resist drawing too many conclusions from Figure 6, but we will say that Ce··Ce distances in **4** are on average longer than in smaller MNPs. This is also seen in the Ce··Ce ranges for **1** (Ce_{24}), **2** (Ce_{38}) and **4** (Ce_{100}) of 3.65–3.86 Å, 3.57–3.86 Å, and 3.51–4.03 Å, respectively, that is, there are few Ce··Ce distances in **1** and **2** equal or greater than that in bulk ceria (3.83 Å).

Additionally, for **1** and **4** the average surface-to-body Ce··Ce distance is slightly shorter than the average body-to-body one indicating a relaxation of the surface Ce atoms towards the core to reduce the total surface free energy.[43] Complex **2**, which adopts a higher symmetry truncated-octahedron morphology that is energetically favorable for CNPs, has the opposite trend; the average body-to-body distance is slightly shorter than the average surface-to-body distance. To explore all these trends further, we will need to expand the family to several other large nuclearities both smaller and greater than **4**.

The UV/Vis spectra of **4**–**7** in DMF in the 200–800 nm range (Supporting Information, Figure S6) are similar, all showing a peak at about 270 nm and rather featureless profiles at higher wavelengths. Complex **4** has a greater absorbance between 285–320 nm that can be attributed to its greater number of Ce^{4+} ions.[44–46]

Conclusion

The family of MNPs of CeO_2 has been successfully expanded to a $\{Ce_{100}O_{167}\}$ core atom count and a longest dimension of 2.4 nm, both much higher than seen for the other members of the family. As a result, **4** has several larger facet sizes than observed in the smaller MNPs, but otherwise its surface features are very similar to those in the latter, suggesting by extrapolation that they are truly providing structural insights to atomic resolution into the surfaces of ultra-small CNPs. Notably, the average body Ce···Ce distances in the core of **4** are already essentially identical to those of bulk ceria, an observation we had not seen for the smaller members of the family, which are too small to have any significant amount of body Ce atoms. We are thus optimistic that **4** is the first member of a new size regime of MNPs of CeO_2 that are more analogous to ultra-small CNPs and will permit more informative comparisons as a result. Additional high nuclearity members are therefore currently being sought.

Acknowledgements

We thank the NSF for funding this work through grant CHE-1900321, and for the purchase of the X-ray diffractometer through grant CHE-1828064

Conflict of interest

The authors declare no conflict of interest.

Keywords: atomic precision · cerium · cluster compounds · molecular nanoparticle · nanoceria

[1] A. Trovarelli, J. Llorca, *ACS Catal.* **2017**, *7*, 4716–4735.
[2] A. Trovarelli, *Catal. Rev.* **1996**, *38*, 439–520.
[3] Q. Wang, B. Zhao, G. Li, R. Zhou, *Environ. Sci. Technol.* **2010**, *44*, 3870–3875.
[4] K. Reed, A. Cormack, A. Kulkarni, M. Mayton, D. Sayle, F. Klaessig, B. Stadler, *Environ. Sci. Nano* **2014**, *1*, 390–405.
[5] M. Flytzani-Stephanopoulos, *MRS Bull.* **2001**, *26*, 885–889.
[6] N. Jaiswal, K. Tanwar, R. Suman, D. Kumar, S. Upadhyay, O. Parkash, *J. Alloys Compd.* **2019**, *781*, 984–1005.
[7] M. Melchionna, P. Fornasiero, *Mater. Today* **2014**, *17*, 349–357.
[8] M. Das, S. Patil, N. Bhargava, J.-F. Kang, L. M. Riedel, S. Seal, J. J. Hickman, *Biomaterials* **2007**, *28*, 1918–1925.
[9] S. Das, J. M. Dowding, K. E. Klump, J. F. McGinnis, W. Self, S. Seal, *Nanomedicine* **2013**, *8*, 1483–1508.

 © 2021 Wiley-VCH GmbH

[10] S. Kargozar, F. Baino, S. J. Hoseini, S. Hamzehlou, M. Darroudi, J. Verdi, L. Hasanzadeh, H.-W. Kim, M. Mozafari, *Nanomedicine* **2018**, *13*, 3051 – 3069.
[11] N. Thakur, P. Manna, J. Das, *J. Nanobiotechnol.* **2019**, *17*, 84.
[12] S. Carrettin, P. Concepción, A. Corma, J. M. López Nieto, V. F. Puntes, *Angew. Chem. Int. Ed.* **2004**, *43*, 2538 – 2540; *Angew. Chem.* **2004**, *116*, 2592 – 2594.
[13] H. S. Nanda, *RSC Adv.* **2016**, *6*, 111889 – 111894.
[14] Y.-Y. Tsai, J. Oca-Cossio, K. Agering, N. E. Simpson, M. A. Atkinson, C. H. Wasserfall, I. Constantinidis, W. Sigmund, *Nanomedicine* **2007**, *2*, 325 – 332.
[15] R. A. Yokel, M. T. Tseng, M. Dan, J. M. Unrine, U. M. Graham, P. Wu, E. A. Grulke, *Nanomed. Nanotechnol. Biol. Med.* **2013**, *9*, 398 – 407.
[16] A. Asati, S. Santra, C. Kaittanis, J. M. Perez, *ACS Nano* **2010**, *4*, 5321 – 5331.
[17] J. M. Dowding, S. Das, A. Kumar, T. Dosani, R. McCormack, A. Gupta, T. X. T. Sayle, D. C. Sayle, L. von Kalm, S. Seal, W. T. Self, *ACS Nano* **2013**, *7*, 4855 – 4868.
[18] J. Gagnon, K. M. Fromm, *Eur. J. Inorg. Chem.* **2015**, 4510 – 4517.
[19] K. J. Mitchell, K. A. Abboud, G. Christou, *Nat. Commun.* **2017**, *8*, 1445.
[20] K. J. Mitchell, J. Goodsell, B. Russell-Webster, U. Twahir, A. Angerhofer, K. A. Abboud, G. Christou, *Inorg. Chem.* **2021**, *60*, 1641 – 1653.
[21] B. Russell-Webster, K. A. Abboud, G. Christou, *Chem. Commun.* **2020**, *56*, 5382 – 5385.
[22] Z. L. Wang, X. Feng, *J. Phys. Chem. B* **2003**, *107*, 13563 – 13566.
[23] Z. Liu, X. Li, M. Mayyas, P. Koshy, J. N. Hart, C. C. Sorrell, *CrystEngComm* **2017**, *19*, 4766 – 4776.
[24] J. C. Conesa, *Surf. Sci.* **1995**, *339*, 337 – 352.
[25] T. X. T. Sayle, S. C. Parker, C. R. A. Catlow, *Surf. Sci.* **1994**, *316*, 329 – 336.
[26] T. X. T. Sayle, M. Molinari, S. Das, U. M. Bhatta, G. Möbus, S. C. Parker, S. Seal, D. C. Sayle, *Nanoscale* **2013**, *5*, 6063 – 6073.
[27] T. Montini, M. Melchionna, M. Monai, P. Fornasiero, *Chem. Rev.* **2016**, *116*, 5987 – 6041.
[28] Crystallographic data for [**4**]$(PhCO_2)_8(NO_3)_8$ are provided in the Supporting Information. Deposition Number 2067840 contain the supplementary crystallographic data for this paper. These data are provided free of charge by the joint Cambridge Crystallographic Data Centre and Fachinformationszentrum Karlsruhe Access Structures service www.ccdc.cam.ac.uk/structures.
[29] A. Müller, P. Gouzerh, *Chem. Soc. Rev.* **2012**, *41*, 7431 – 7463.
[30] S. Bestgen, O. Fuhr, B. Breitung, V. S. K. Chakravadhanula, G. Guthausen, F. Hennrich, W. Yu, M. M. Kappes, P. W. Roesky, D. Fenske, *Chem. Sci.* **2017**, *8*, 2235 – 2240.
[31] T. Higaki, M. Zhou, K. J. Lambright, K. Kirschbaum, M. Y. Sfeir, R. Jin, *J. Am. Chem. Soc.* **2018**, *140*, 5691 – 5695.
[32] T. Higaki, M. Zhou, G. He, S. D. House, M. Y. Sfeir, J. C. Yang, R. Jin, *Proc. Natl. Acad. Sci. USA* **2019**, *116*, 13215 – 13220.
[33] C. Kumara, X. Zuo, J. Ilavsky, D. Cullen, A. Dass, *J. Phys. Chem. C* **2015**, *119*, 11260 – 11266.
[34] I. D. Brown, *Chem. Rev.* **2009**, *109*, 6858 – 6919.
[35] N. E. Brese, M. O'Keeffe, *Acta Crystallogr. Sect. B* **1991**, *47*, 192 – 197.
[36] M. Molinari, S. C. Parker, D. C. Sayle, M. S. Islam, *J. Phys. Chem. C* **2012**, *116*, 7073 – 7082.
[37] R. K. Hailstone, A. G. DiFrancesco, J. G. Leong, T. D. Allston, K. J. Reed, *J. Phys. Chem. C* **2009**, *113*, 15155 – 15159.
[38] A. E. Baranchikov, O. S. Polezhaeva, V. K. Ivanov, Y. D. Tretyakov, *CrystEngComm* **2010**, *12*, 3531 – 3533.
[39] S. Tsunekawa, J.-T. Wang, Y. Kawazoe, *J. Alloys Compd.* **2006**, *408 – 412*, 1145 – 1148.
[40] D. Prieur, W. Bonani, K. Popa, O. Walter, K. W. Kriegsman, M. H. Engelhard, X. Guo, R. Eloirdi, T. Gouder, A. Beck, T. Vitova, A. C. Scheinost, K. Kvashnina, P. Martin, *Inorg. Chem.* **2020**, *59*, 5760 – 5767.
[41] L. Chen, P. Fleming, V. Morris, J. D. Holmes, M. A. Morris, *J. Phys. Chem. C* **2010**, *114*, 12909 – 12919.
[42] C. Loschen, S. T. Bromley, K. M. Neyman, F. Illas, *J. Phys. Chem. C* **2007**, *111*, 10142 – 10145.
[43] M. Sterrer, H.-J. Freund, *Surface and Interface Science*, Wiley, Hoboken, **2013**, pp. 229 – 278.
[44] E. G. Heckert, A. S. Karakoti, S. Seal, W. T. Self, *Biomaterials* **2008**, *29*, 2705 – 2709.
[45] A. Paul, M. Mulholland, M. S. Zaman, *J. Mater. Sci.* **1976**, *11*, 2082 – 2086.
[46] S. Tsunekawa, T. Fukuda, A. Kasuya, *J. Appl. Phys.* **2000**, *87*, 1318 – 1321.

Manuscript received: March 2, 2021
Accepted manuscript online: March 26, 2021
Version of record online: April 26, 2021

 © 2021 Wiley-VCH GmbH